

Communication

Propagation Properties of Generalized Schell-Model Pulse Sources in Dispersive Media

Xiayin Liu ^{*}, Zhiyu Cai, Xiaogang Wang and Bijun Xu 

Department of Physics, Zhejiang University of Science and Technology, Hangzhou 310023, China; 211909702005@zust.edu.cn (Z.C.); wxg1201@zust.edu.cn (X.W.); xubijun@zust.edu.cn (B.X.)

^{*} Correspondence: liuxy@zust.edu.cn

Abstract: A model of a generalized pulse source, whose complex degree of temporal coherence is described by a function of the n th power difference of two instants, was constructed. As examples, we consider the generalized Gaussian and multi-Gaussian Schell-model pulse sources and study their propagation in dispersive media. It is indicated that such pulse beams present unique self-focusing, off-axis self-shifting and asymmetric self-splitting characteristics by adjusting the power exponent and phase parameters. Further, we explicitly discuss how the coherence time, summation factor as well as the dispersive coefficient significantly affect the self-focusing and self-shifting behaviors of the pulse beam. The results will benefit some applications involving pulse shaping, optical trapping and remote sensing.

Keywords: complex degree of temporal coherence; pulse beam; phase construction; spectral intensity

1. Introduction

There has been growing interest in the modeling of partially coherent sources with special correlations since a general representation for bona fide coherent sources was introduced [1]. Compared with the conventional Gaussian-correlated Schell-model sources, the function forms describing the complex degree of coherence (CDC) of the special correlated Schell-model source are more diverse, which leads to abundant far-field intensity distribution profiles. For example, there are uniformly partially coherent beams with a spatially varying coherence function generating a self-focusing and laterally self-shifting intensity profile [2] and multi-Gaussian Schell model beams with the correlated function being the summation of multi-Gaussian functions, producing a circular or rectangular flat-topped field [3,4]. When the multi-Gaussian function is replaced by a multi-sinc function, multi-irregular or lattice-like patterns will be generated [5]. Additionally, the spectral density of the Schell-model source with a cosine-Gaussian correlation or Hermite-Gaussian correlation, also exhibits dark-hollow or self-splitting profiles [6,7]. Apart from the modeling of the magnitude of the CDC above, the inclusion of phases in the CDC is also an important method in modulating the propagation features of the optical field. Typical examples include partially coherent beams with a vortex phase and a twisted phase, which have been shown to have significant effects in exploring singular optics, beam rotation and mitigation of turbulence-induced scintillation [8–13]. Recently, a fine Schell-like source model, of which the complex degree of coherence has an even magnitude and odd phase distribution, has been proposed [14]. On its basis, a slew of novel source models were constructed, in which the magnitude and phase structure of the CDC were defined as the function of the n -th power difference of two source points rather than their direct distance. Such unique source models provide a method for generating a self-focusing optical field with a controllable focal length by changing the phase factor [15–20].

Due to the space-time analogy between the spatial coherence properties of partially coherent beams and the temporal counterparts of partially coherent pulses, the temporal



Citation: Liu, X.; Cai, Z.; Wang, X.; Xu, B. Propagation Properties of Generalized Schell-Model Pulse Sources in Dispersive Media. *Photonics* **2023**, *10*, 1378. <https://doi.org/10.3390/photonics10121378>

Received: 9 November 2023

Revised: 11 December 2023

Accepted: 13 December 2023

Published: 14 December 2023



Copyright: © 2023 by the authors. Licensee MDPI, Basel, Switzerland. This article is an open access article distributed under the terms and conditions of the Creative Commons Attribution (CC BY) license (<https://creativecommons.org/licenses/by/4.0/>).

coherence-induced effects on the propagation of unconventional Schell-model pulses have been considered. The models include partially coherent pulses with non-uniform temporal correlations [21], multi Gaussian temporal correlations [22], fractional multi-Gaussian temporal correlations [23], cosine-Gaussian temporal degrees of coherence [24,25], multi-cosine-Gaussian correlations and Laguerre-Gaussian temporal correlations [26,27]. All these pulse sources exhibit extraordinary propagation characteristics in dispersive media and have potential applications in pulse shaping, temporal ghost imaging, and inertial confinement fusion. In addition, the behaviors of twisted space-time partially coherent beams and spatiotemporal vortex pulses carrying an orbital angular momentum were explored both experimentally and theoretically [28–33], which provides guidance on applications related to sculpturing spatiotemporal wave packets and spatiotemporal spin-orbit angular momentum coupling. Recently, spectral phase-modulated pulses trains and phase-structured complex temporal degree of coherence pulse sources were introduced [34–36], which show the nontrivial phase function can be used to control the distribution of the average arrival time of the pulse train. These inspire us to explore the theoretical model of the random pulse with the temporal coherence being the function of the n -th power difference of two instants.

In this manuscript, we introduce the generalized pulse source whose complex degree of temporal coherence is characterized by power-exponent magnitude and phase structures. By taking the generalized Gaussian and multi-Gaussian Schell-model pulse sources as examples, we mainly explore the propagation characteristics of such pulses in dispersive media. The influences of the source and media parameters on the self-focusing and laterally self-shifting behaviors of pulses are illustrated.

2. Theoretical Model

The second-order mutual coherence function (MCF) characterizing the temporal correlation properties of the ensemble of non-stationary pulses has the form [37]

$$\Gamma_0(t_{10}, t_{20}) = \sqrt{I_0(t_{10})} \sqrt{I_0(t_{20})} \gamma_0(t_{10}, t_{20}). \tag{1}$$

In the time domain, in order to be a Hermitian and non-negative definite correlation function, the MCF needs to have the following superposition representation [1]

$$\Gamma_0(t_{10}, t_{20}) = \int p(\nu) H_0^*(t_{10}, \nu) H_0(t_{20}, \nu) d\nu, \tag{2}$$

where function $p(\nu)$ is a real and non-negative weight function, and $H_0(t, \nu)$ is an arbitrary kernel function, chosen as a Fourier-like form

$$H_0(t, \nu) = \alpha(t) \exp(-2\pi i \nu \cdot f(t)). \tag{3}$$

Here, $\alpha(t)$ denotes the complex amplitude profile. $f(t)$ is a real function. In view of Equations (2) and (3), the MCF is given by

$$\Gamma_0(t_{10}, t_{20}) = \alpha^*(t_{10}) \alpha(t_{20}) \mathcal{F}[f(t_{10}) - f(t_{20})], \tag{4}$$

where $\mathcal{F}[f(t_{10}) - f(t_{20})] = \mathcal{F}[\gamma(t_d)] = p(\nu)$.

Then, the MCF is obtained as the form

$$\Gamma_0(t_{10}, t_{20}) = \alpha^*(t_{10}) \alpha(t_{20}) \gamma(t_d). \tag{5}$$

The function $\alpha(t)$ is set to the Gaussian

$$\alpha(t) = \exp\left[-t^2/T_0^2\right], \tag{6}$$

with T_0 being the pulse width. Equation (4) implies that the intensity profile of the propagating pulse mainly depends on the choice of the function $f(t)$. If $f(t)$ is a linear function of time, Equation (4) stands for the conventional Schell-model pulse source. In this manuscript, we set $f(t)$ as a power function of time

$$f(t) = t^n. \tag{7}$$

Then, the MCF takes the form

$$\Gamma_0(t_{10}, t_{20}) = \exp\left[-\frac{t_{10}^2 + t_{20}^2}{T_0^2}\right] \gamma(t_{10}^n - t_{20}^n), \tag{8}$$

where $\gamma(t_d)$ is the complex degree of temporal coherence (CDTC), $t_d = t_1^n - t_2^n$. Following references [14,15,17], $\gamma(t_d)$ can be expressed as the self-convolution of a sliding temporal function $g(t_d)$

$$\gamma(t_d) = g(t_d) \otimes g(t_d), \tag{9}$$

where \otimes stands for convolution.

$$g(t_d) = g_M(t_d) \exp(ig_P(t_d)). \tag{10}$$

The sliding function $g(t_d)$ needs to be a Hermitian function, so it has an even real part $g_M(t_d)$ and an odd imaginary part $g_P(t_d)$.

3. Propagation of the Generalized Schell-Model Pulses in Dispersive Media

3.1. Generalized Gaussian Schell-Model Pulse

Let us now set $g_M(t_d)$ as a Gaussian temporal function

$$g_M(t_d) = \left(\sqrt{T_c^n \sqrt{\pi}}\right)^{-1} \exp\left[-t_d^2 / (2T_c^{2n})\right], \tag{11}$$

where T_c is the coherence time. The linear phase is set as

$$g_P(t_d) = a^n t_d, \tag{12}$$

in which $a = a_0/10^{-12}$, and a_0 is real constant; therefore, the sliding function takes the form

$$g(t_d) = \left(\sqrt{T_c^n \sqrt{\pi}}\right)^{-1} \exp\left[-t_d^2 / (2T_c^{2n}) + ia^n t_d\right]. \tag{13}$$

Inserting from Equation (13) into Equation (9), we obtain the corresponding expression of CDTC.

$$\gamma(t_{10}, t_{20}) = \exp\left[-\frac{(t_{10}^n - t_{20}^n)^2}{4T_c^{2n}} + ia^n(t_{10}^n - t_{20}^n)\right]. \tag{14}$$

Hence, the MCF is given by the form

$$\Gamma_0(t_{10}, t_{20}) = \exp\left(-\frac{t_{10}^2 + t_{20}^2}{T_0^2}\right) \exp\left[-\frac{(t_{10}^n - t_{20}^n)^2}{4T_c^{2n}} + ia^n(t_{10}^n - t_{20}^n)\right]. \tag{15}$$

Equation (15) represents a generalized Gaussian Schell-model pulse source.

Figure 1 illustrates the magnitude of the complex degree of temporal coherence of the pulse source and the corresponding phase for the different power order n . It can be found that the magnitude of the CDTC features diagonal symmetry when n takes odd numbers and Cartesian symmetry for even numbers. When $n = 2$, the cross-like shape is similar to the profile of the degree of coherence of non-uniformly correlated pulses [21]. With the order n increasing, the magnitude of the temporal correlation of the pulse remains

the same around the temporal center. In addition, Figure 1(b1–b4) show the corresponding contour profile of the phase structure. Although the contour of the phase is similar to that of the magnitude, the phase increases along the contour profile from $-\pi$ to π , and the number of phase envelopes depends on the values of n , which is different from that of the spatiotemporal coherency vortex whose phase increases along a spiral line from $-\pi$ to π [33].

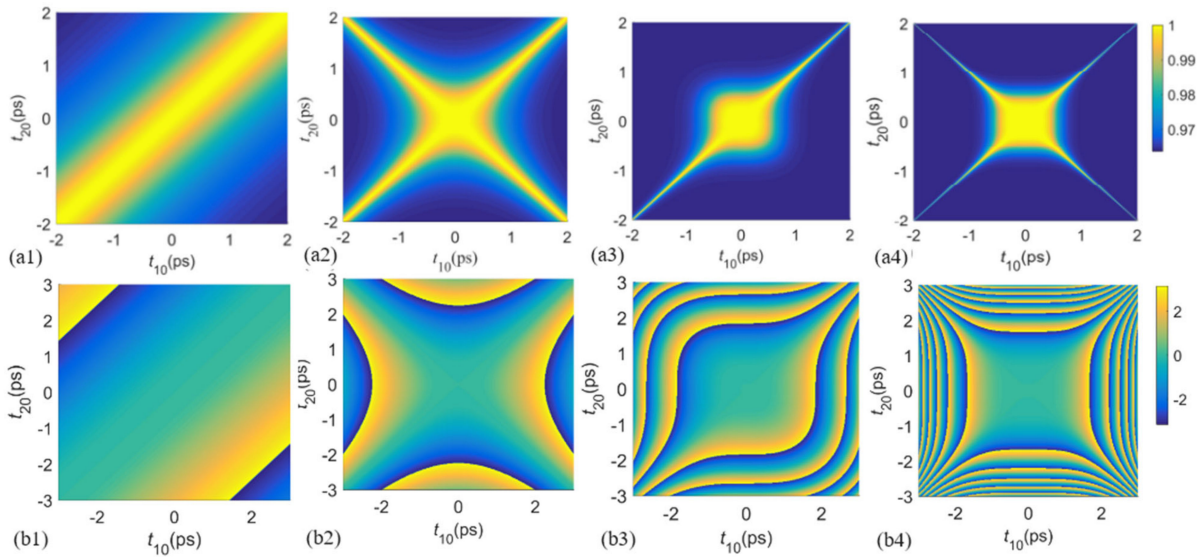


Figure 1. (a1–a4) Magnitude of CDTC for different exponent values. (a1) $n = 1$; (a2) $n = 2$; (a3) $n = 3$; (a4) $n = 4$. (b1–b4) The corresponding phase of CDTC for $a = 2/5\pi$.

The propagation formula of such a pulse from the source plane $z = 0$ to a plane $z > 0$ in a dispersive medium can be expressed by the temporal counterpart of the generalized Huygens–Fresnel integral [37].

$$\Gamma(t_1, t_2, z) = \frac{1}{2\pi\beta_2 z} \iint \Gamma^{(0)}(t_{10}, t_{20}) \times \exp\left\{\frac{i}{2\beta_2 z} [(t_{10}^2 - t_{20}^2) - 2(t_{10}t_1 - t_{20}t_2) + (t_1^2 - t_2^2)]\right\} dt_{10} dt_{20} \quad (16)$$

where β_2 represents the group velocity dispersion coefficient. On inserting from Equation (15) into Equation (16), the MCF of the pulse beam on propagation in dispersive media can be obtained

$$\Gamma(t_1, t_2, z) = \frac{1}{2\pi\beta_2 z} \exp\left[\frac{i}{2\pi\beta_2 z} (t_1^2 - t_2^2)\right] \iint F_t dt_{10} dt_{20}, \quad (17)$$

where

$$F_t = \exp\left[-\frac{t_{10}^2 + t_{20}^2}{4T_0^2} - \frac{(t_{10}^n - t_{20}^n)^2}{4T_c^{2n}} + ia^n(t_{10}^n - t_{20}^n) + \frac{i}{2\beta_2 z} (t_{10}^2 - t_{20}^2 - 2t_{10}t_1 + 2t_{20}t_2)\right]. \quad (18)$$

The source and media parameters are chosen to be $T_0 = 1\text{ps}$, $T_c = 0.7\text{ps}$, $\beta = 50\text{ps}^2\text{km}^{-1}$.

Figure 2 mainly explores the effects of different values of the power exponent n on the evolution of the intensity of the pulse on propagation in dispersive media when neglecting the phase term, i.e., $a = 0$. When $a = 0$ and $n = 1$, Equation (17) corresponds to conventional Gaussian Schell-model pulses, so the intensity distribution exhibits a Gaussian shape as shown in Figure 1a. When $n > 1$, the pulse beams present a self-focusing phenomenon in the intermediate field. Moreover, as the values of n increase, a self-splitting pulse appears in the near field.

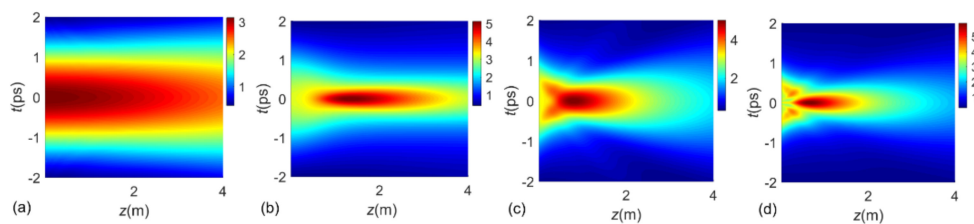


Figure 2. Intensity evolution of the generalized Gaussian Schell-model pulse with a trivial phase ($a = 0$). (a) $n = 1$; (b) $n = 2$; (c) $n = 3$; (d) $n = 4$.

From Figure 2 it can be seen that the self-focusing behaviors of such pulse beams are closely related with the values of the exponent n . Particularly, when $n = 2$, the self-focusing effect is evident. In this case, how the self-focusing behaviors are affected by the dispersion coefficient β_2 and the coherence time T_C are further studied in Figure 3. As β_2 increases, the self-focusing length reduces and the position of the maximum intensity of the pulse is closer to pulse source, but the maximum intensity remains the same. On increasing the coherence time T_C , the situation becomes the opposite. The self-focusing length increases, the maximum intensity declines and the corresponding position is further from the pulse source.

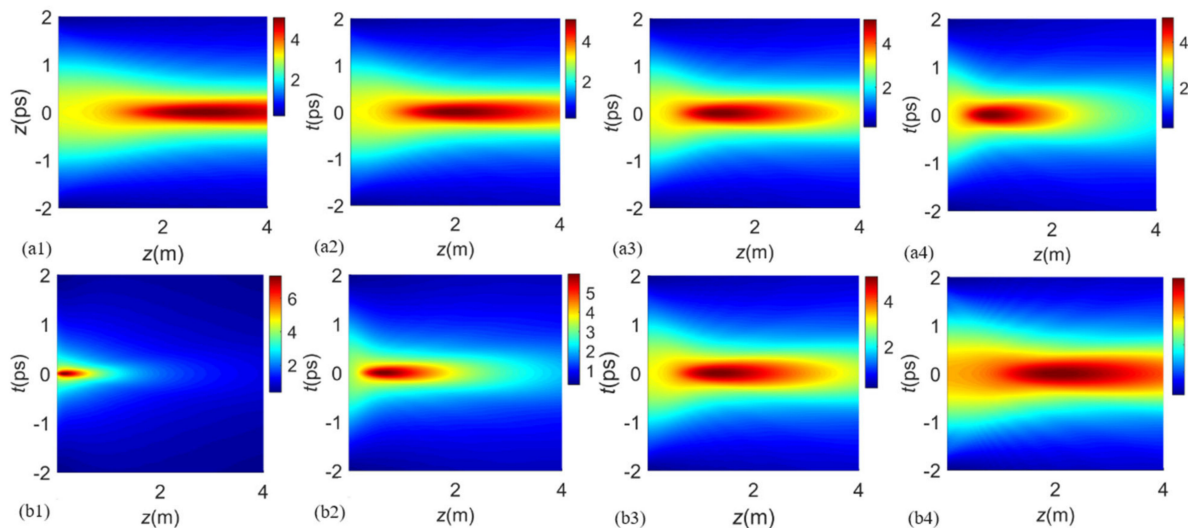


Figure 3. Intensity distribution for different values of β_2 and T_C ($n = 2, a = 0$). (a1–a4) 25 ps²/km, 35 ps²/km; 50 ps²/km; 75 ps²/km; (b1–b4), 0.3ps; 0.5ps; 0.7ps; 0.9ps.

Figure 4 presents the evolutions of pulses with a non-trivial phase. Figure 4a,c show that the composition of the phase and the exponent n being odd result in the pulse ensemble’s shift along the temporal axis, which is analogous to the behaviors of non-uniformly correlated partially coherent pulses upon propagation in dispersive media [21]. In particular, when $n = 3$, the evolution of the pulse intensity follows a parabola-like trajectory. Though there is no shift in the maximum intensity with n being even as Figure 4b,d indicate, the maximum intensity increases and the position approaches the pulse source in comparison with Figure 2b,d.

Figure 5 further illustrates the influences of different values of dispersion coefficient β_2 , coherence time T_C as well as phase parameter a on the self-shifting of the pulse intensity along the t -axis. It is shown that the phase parameter has a more significant impact on the shift than the other two parameters, β_2 and T_C . With T_C being smaller, the intensity of the pulse attenuates quickly along the z -axis. When $a = \pi/5$, the slightly asymmetric distribution of pulse intensity closer to the pulse source appears. As a increases, the maximum intensity of the pulse increases and the self-shifting effect is more evident.

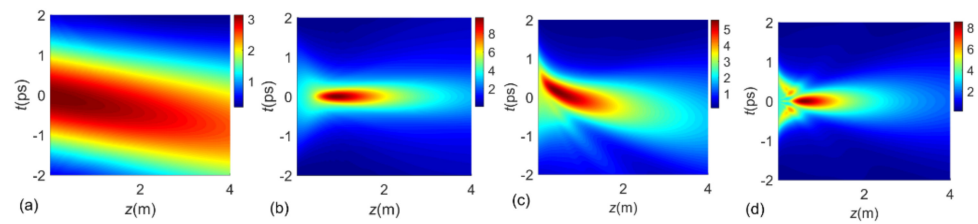


Figure 4. Intensity evolution of the generalized Gaussian Schell-model pulse with a non-trivial phase. Same as Figure 2 except for $a = 2/5\pi$.

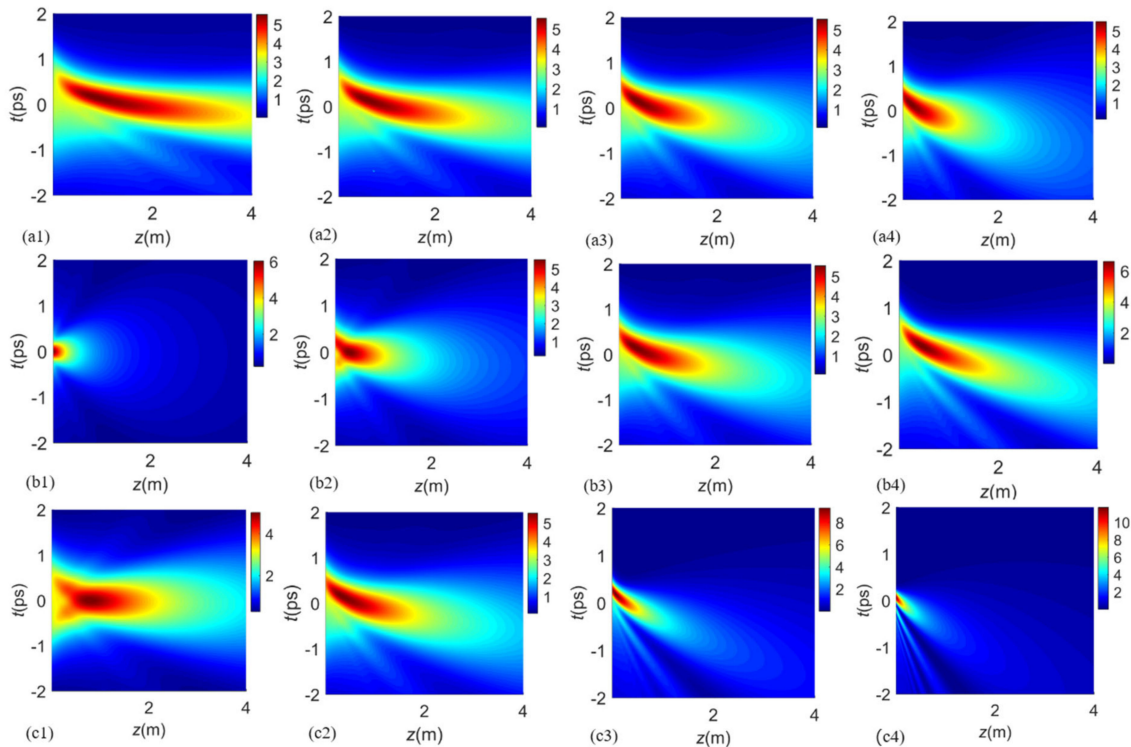


Figure 5. (a1–b4) Same as Figure 3 except for $n = 3, a = 2/5\pi$. Figure 5 (c1–c4) Intensity distribution for different values of a . (c1) $1/5\pi$; (c2) $2/5\pi$; (c3) $3/5\pi$; (c4) $4/5\pi$.

In Figure 6, the intensity evolution of the pulse center along the z direction and the transverse cross-section of the intensity of the pulse versus time t at the distance $z = 1$ m are presented for different values of phase parameter a , dispersion coefficient β and coherent time T_C . Figure 6(a1,c1) show that the position of the maximum pulse is closer to pulse source with increasing a and reducing T_C . The original pulse displays asymmetric splitting along the t -axis and the number of sub-pulses increases as Figure 6(a2,c2) show. Figure 6(b1) indicates that the intensity of the center pulse is invariant for different values of the dispersion coefficient, which is consistent with that in Figure 5(a1–a4). At the propagation distance $z = 1$ m, for larger values of β_2 or a , and smaller values of T_C , a further shift away from the z -axis is generated. At the same time, the pulse intensity declines, which is caused by the reduction in the focusing length.

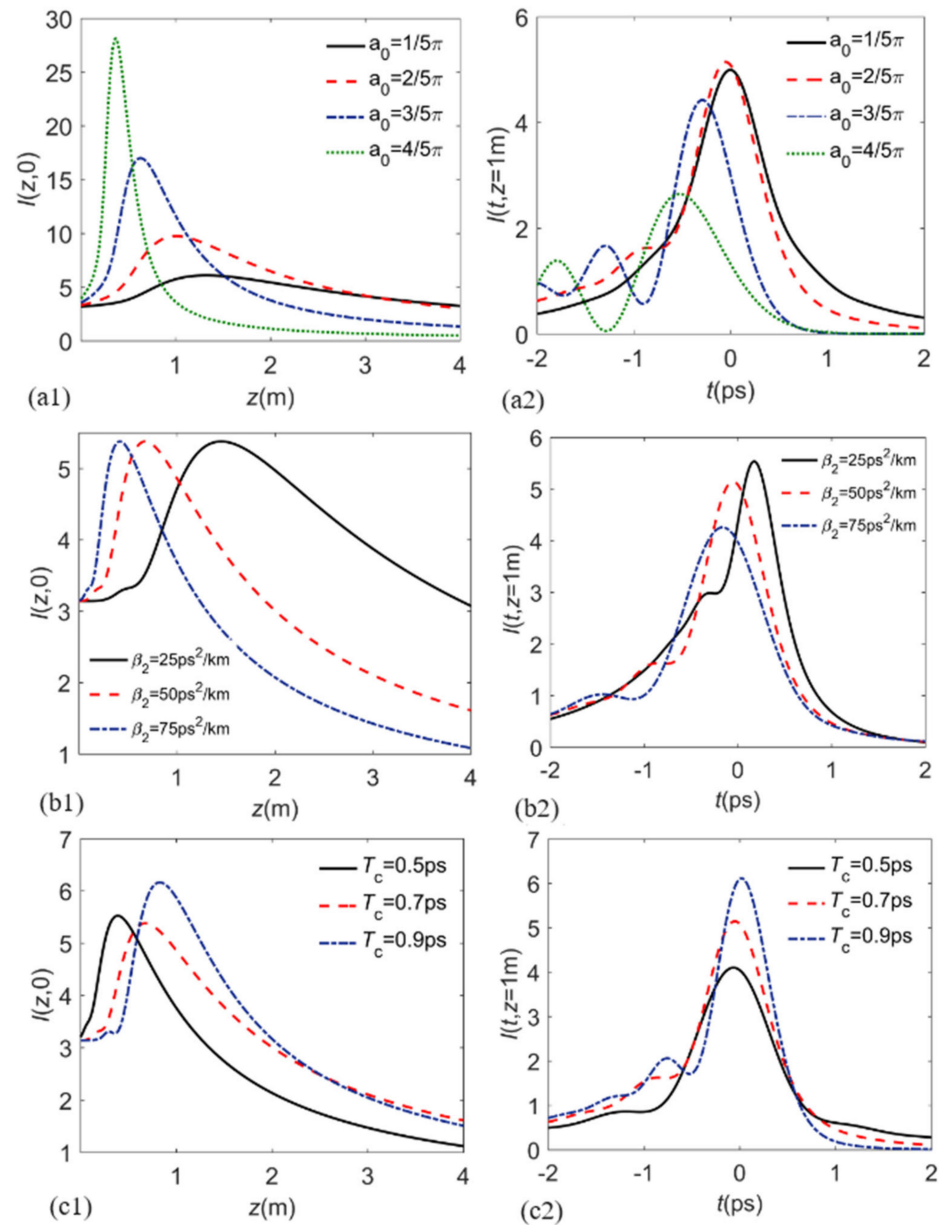


Figure 6. (a1,b1,c1) Changes of maximum of pulse intensity along the z direction for different values of a_0 , β_2 and T_c and (a2,b2,c2) pulse shapes at the propagation distance $z = 1\text{ m}$ ($n = 3$).

3.2. Generalized Multi-Gaussian Schell-Model Pulse

As an extension of the source model above, we now express the CDTC as a linear superposition of multiple self-convolutions of a sliding temporal function $g(t_d)$

$$\gamma(t_d) = \frac{1}{C_0} \sum_{m=1}^M \frac{(-1)^{m-1}}{\sqrt{m}} \binom{M}{m} [g_m(t_d) \otimes g_m(t_d)], \tag{19}$$

where C_0 is the normalization factor

$$C_0 = \sum_{m=1}^M \frac{(-1)^{m-1}}{\sqrt{m}} \binom{M}{m}. \tag{20}$$

The sliding function takes the form

$$g_m(t_d) = \left(\sqrt{T_c^n \sqrt{m\pi}} \right)^{-1} \exp \left[-t_d^2 / \left(2mT_c^{2n} \right) + ia^n t_d \right]. \tag{21}$$

Thus, the CDTC can be expressed as

$$\gamma(t_{10}, t_{20}) = \frac{1}{C_0} \sum_{m=1}^M \frac{(-1)^{m-1}}{\sqrt{m}} \binom{M}{m} \exp \left[-\frac{(t_{10}^n - t_{20}^n)^2}{4mT_c^{2n}} + ia^n (t_{10}^n - t_{20}^n) \right]. \tag{22}$$

Then, the MCF of the generalized multi-Gaussian Schell model pulse source can be obtained

$$\Gamma_0(t_{10}, t_{20}) = \frac{1}{C_0} \exp \left(-\frac{t_{10}^2 + t_{20}^2}{4T_0^2} \right) \times \sum_{m=1}^M \frac{(-1)^{m-1}}{\sqrt{m}} \binom{M}{m} \exp \left[-\frac{(t_{10}^n - t_{20}^n)^2}{4mT_c^{2n}} + ia^n (t_{10}^n - t_{20}^n) \right]. \tag{23}$$

Inserting from Equation (23) into Equation (16), the average intensity of the pulse at the propagation distance z takes the integral form and can be evaluated numerally.

$$I(t, z) = \frac{1}{2\pi\beta_2 z C_0} \iint F(t_{10}, t_{20}, t, z) dt_{10} dt_{20}, \tag{24}$$

where

$$F(t_{10}, t_{20}, t, z) = \exp \left[-\frac{t_{10}^2 + t_{20}^2}{4T_0^2} + \frac{i}{2\beta_2 z} (t_{10}^2 - t_{20}^2 - 2t(t_{10} - t_{20})) \right] \times \sum_{m=1}^M \frac{(-1)^{m-1}}{\sqrt{m}} \binom{M}{m} \exp \left[-\frac{(t_{10}^n - t_{20}^n)^2}{4mT_c^{2n}} + ia^n (t_{10}^n - t_{20}^n) \right] \tag{25}$$

Figures 7 and 8 mainly explore the transverse cross-section of the intensity of the generalized multi-Gaussian pulse at the special propagation distance $z = 1.5$ m for different source and media parameters. When $M = 20$ and $n = 1$, flat-topped pulse profiles are formed and shift laterally along the temporal axis as Figure 7a indicates. But when $n > 1$, the flat-topped profile is reshaped due to the self-focusing effect. Figures 7b and 7c show, respectively, that the pulse maxima are different for different values of M . In Figure 8(a1), when $M = 20$, $n = 1$ and $a = 0$, the generated flat-topped pattern is in good agreement with that of the multi Gaussian Schell-model pulse [22]. With increasing a , the flat-topped profile laterally shifts but the shape remains the same. However, for different values of β_2 and T_C , not only does the pulse profile shift, but also its shape changes. Figure 8(b1–b3) reveal that for smaller values of β_2 or larger T_C , the maximum intensity of the pulse increases. Clearly, the intensity patterns of a generalized multi-Gaussian Schell-model pulse beam can be modified by controlling the source parameters M , a , n and dispersive coefficient β_2 .

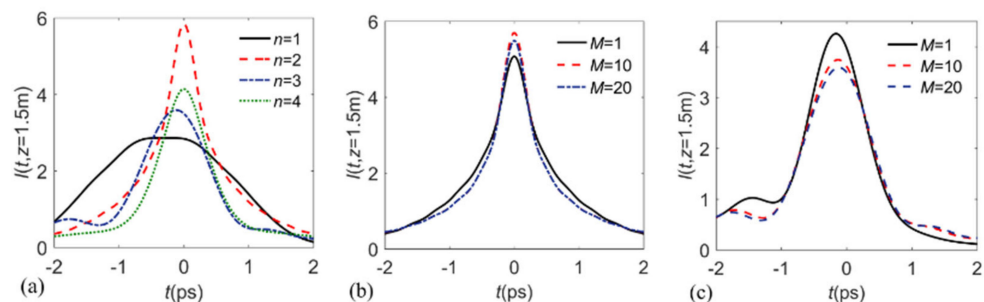


Figure 7. Intensity distributions of the generalized multi-Gaussian Schell-model pulse for different values of M and n at the propagation distance $z = 1.5$ m, (a) $M = 20$; (b) $n = 2$; (c) $n = 3$.

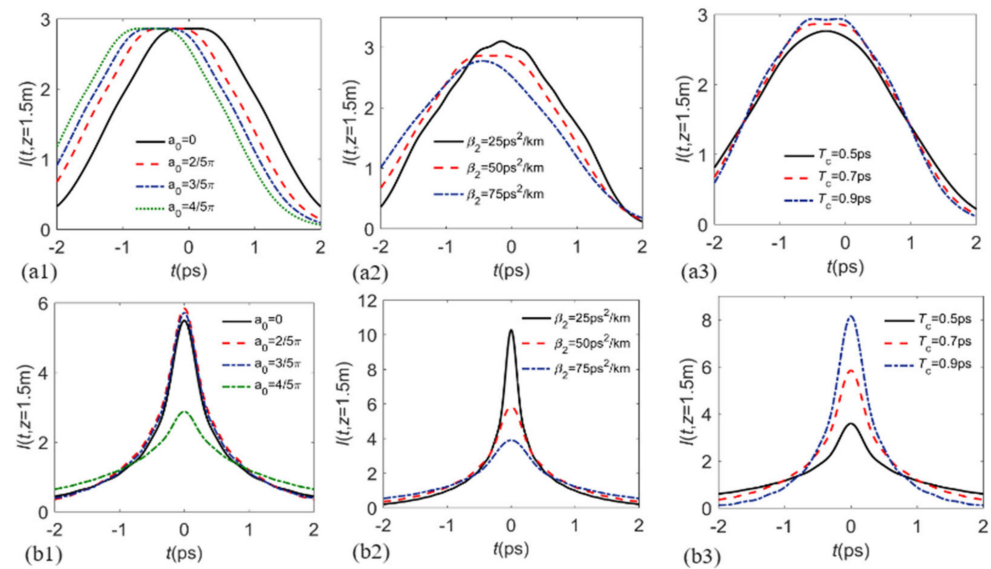


Figure 8. Intensity distributions of the generalized multi-Gaussian Schell-model pulse for different values of a , β_2 and T_c ($M = 20$), (a1–a3) $n = 1$; (b1–b3) $n = 2$.

4. Conclusions

In this manuscript, a generalized pulse source, as a temporal counterpart of a complex Schell-model source with power-exponent magnitude and phase structures, was introduced. The temporal complex degree of coherence of such a pulse source is a function of the n th power difference of time instants. We mainly considered generalized Gaussian and multi-Gaussian Schell-model pulse sources and explored their intensity evolutions in dispersive media. It was demonstrated that the self-focusing effect of the pulse beam is mainly dependent on the power exponent n ($n > 1$). When n is odd and the phase parameter a is nonzero, lateral self-shifting along the t -axis occurs. And for larger values of a , the self-shifting effect is more obvious and the asymmetric self-splitting of the original pulse appears in the near field. Both the coherent time and the dispersive coefficient also have a significant impact on the self-focusing and self-shifting behaviors. In particular, the self-focusing length of the pulse and the position of the pulse maximum can be adjusted by changing the values of the coherent time and the dispersive coefficient. Moreover, for a generalized multi-Gaussian Schell-model pulse, a flat-topped profile is generated when $n = 1$. The flat profile shifts along the t -axis, but the flat width of the pulse center remains invariant with an increasing a . In the case where $n > 1$, due to the self-focusing effect, the flat-topped pattern is reshaped.

The results presented above show that the power-exponent amplitude and phase structures of the CDTC of the generalized pulse source lead to a self-focusing effect and the self-shifting of the maximum intensity of the pulse, which offers a unique method for manipulating the propagation features of pulsed fields and will benefit applications in pulse shaping, optical trapping and manipulation and remote sensing.

Author Contributions: X.L. conceived of and wrote the paper; X.L. and Z.C. performed the numerical simulations; X.L., X.W. and B.X. analyzed and evaluated the results. All authors have read and agreed to the published version of the manuscript.

Funding: This work was supported by the National Natural Science Foundation of China (NSFC) (11604299).

Institutional Review Board Statement: Not applicable.

Informed Consent Statement: Not applicable.

Data Availability Statement: No new data were created or analyzed in this study. Data sharing is not applicable to this article.

Conflicts of Interest: The authors declare no conflict of interest.

References

1. Gori, F.; Santarsiero, M. Devising genuine spatial correlation function. *Opt. Lett.* **2007**, *32*, 3531–3533. [[CrossRef](#)] [[PubMed](#)]
2. Lajunen, H.; Saastamoinen, T. Propagation characteristics of partially coherent beams with spatially varying correlations. *Opt. Lett.* **2011**, *36*, 4104–4106. [[CrossRef](#)] [[PubMed](#)]
3. Sahin, S.; Korotkova, O. Light sources generating far fields with tunable flat profiles. *Opt. Lett.* **2012**, *37*, 2970–2972. [[CrossRef](#)] [[PubMed](#)]
4. Korotkova, O. Random sources for rectangular far fields. *Opt. Lett.* **2014**, *39*, 64–67. [[CrossRef](#)] [[PubMed](#)]
5. Mei, Z.R.; Mao, Y.H. Multi-sinc Schell-model beams and the interaction with a linear random medium. *Laser Phys. Lett.* **2015**, *12*, 095002. [[CrossRef](#)]
6. Mei, Z.R.; Korotkova, O. Cosine-Gaussian Schell-model sources. *Opt. Lett.* **2013**, *38*, 2578–2580. [[CrossRef](#)] [[PubMed](#)]
7. Chen, Y.H.; Gu, J.X.; Wang, F.; Cai, Y.J. Self-splitting properties of a Hermite-Gaussian correlated Schell-model beam. *Phys. Rev. A* **2015**, *91*, 013823. [[CrossRef](#)]
8. Bogatyryova, G.V.; Fel' de, C.V.; Polyanskii, P.V.; Ponomarenko, S.A.; Soskin, M.S.; Wolf, E. Partially coherent vortex beams with a separable phase. *Opt. Lett.* **2003**, *28*, 878–880. [[CrossRef](#)]
9. Palacios, D.M.; Maleev, I.D.; Marathay, A.S.; Swartzlander, G. Spatial correlation singularity of a vortex field. *Phys. Rev. Lett.* **2004**, *92*, 143905. [[CrossRef](#)]
10. Liu, X.L.; Shen, Y.; Liu, L.; Wang, F.; Cai, Y.J. Experimental demonstration of vortex phase-induced reduction in scintillation of a partially coherent beam. *Opt. Lett.* **2013**, *38*, 5323–5326. [[CrossRef](#)]
11. Borghi, R. Twisting partially coherent light. *Opt. Lett.* **2018**, *43*, 1627–1630. [[CrossRef](#)] [[PubMed](#)]
12. Wang, F.; Cai, Y.J.; Eyyuboglu, H.T.; Baykal, Y. Twist phase-induced reduction in scintillation of a partially coherent beam in turbulent atmosphere. *Opt. Lett.* **2012**, *37*, 184–186. [[CrossRef](#)]
13. Wan, L.P.; Zhao, D.M. Controllable rotating Gaussian Schell-model beams. *Opt. Lett.* **2019**, *44*, 735–737. [[CrossRef](#)] [[PubMed](#)]
14. Korotkova, O.; Chen, X. Phase structuring of the complex degree of coherence. *Opt. Lett.* **2018**, *43*, 4727–4730. [[CrossRef](#)] [[PubMed](#)]
15. Chen, X.; Korotkova, O. Phase structuring of the 2D complex coherence states. *Opt. Lett.* **2019**, *44*, 2470–2473. [[CrossRef](#)] [[PubMed](#)]
16. Mei, Z.R.; Korotkova, O. Cross-spectral densities with helical-Cartesian phase. *Opt. Express* **2020**, *28*, 20438–20488. [[CrossRef](#)] [[PubMed](#)]
17. Mei, Z.R. Generalized Schell-model sources. *Opt. Express* **2020**, *28*, 39058–39066. [[CrossRef](#)] [[PubMed](#)]
18. Ata, Y.; Korotkova, O. Electromagnetic phase coherence grating for atmospheric applications. *Opt. Lett.* **2021**, *46*, 5240–5243. [[CrossRef](#)] [[PubMed](#)]
19. Mei, Z.R. Special correlation model sources producing a self-focusing field. *Opt. Express* **2021**, *29*, 25337–25343. [[CrossRef](#)]
20. Mei, Z.R.; Korotkova, O.; Zhao, D.; Mao, Y. Self-focusing vortex beams. *Opt. Lett.* **2021**, *46*, 2384–2387. [[CrossRef](#)]
21. Lajunen, H.; Saastamoinen, T. Non-uniformly correlated partially coherent pulses. *Opt. Express* **2013**, *21*, 190–195. [[CrossRef](#)] [[PubMed](#)]
22. Ding, C.L.; Korotkova, O.; Pan, L.Z. The control of pulse profiles with tunable temporal coherence. *Phys. Lett. A* **2014**, *378*, 1687–1690. [[CrossRef](#)]
23. Liu, H.L.; Hu, Z.H.; Du, Z.H.; Xia, J.; He, A.; Lü, Y.F. Temporal pulse source generating far fields with sharp optical pulse. *Phys. Lett. A* **2021**, *390*, 127102. [[CrossRef](#)]
24. Ding, C.L.; Korotkova, O.; Zhang, Y.T.; Pan, L.Z. Cosine-Gaussian correlated Schell-model pulsed beams. *Opt. Express* **2014**, *22*, 931–942. [[CrossRef](#)] [[PubMed](#)]
25. Wang, X.H.; Tang, J.H.; Wang, Y.H.; Liu, X.; Liang, C.H.; Zhao, L.N.; Hoenders, B.J.; Cai, Y.J.; Ma, P.J. Complex and phase screen methods for studying arbitrary genuine Schell-model partially coherent pulses in nonlinear media. *Opt. Express* **2022**, *30*, 24222–24231. [[CrossRef](#)]
26. Liu, H.L.; Du, Z.H.; Li, Y.Z.; Chen, H.; Lü, Y.F. Self-focusing and self-splitting properties of partially coherent temporal pulses propagating in dispersive media. *Opt. Express* **2023**, *31*, 7336–7350. [[CrossRef](#)] [[PubMed](#)]
27. Ding, C.L.; Koivurova, M.; Turunen, J.; Pan, L.Z. Temporal self-splitting of optical pulses. *Phys. Rev. A* **2018**, *97*, 053838. [[CrossRef](#)]
28. Bliokh, K.Y. Spatiotemporal vortex pulses: Angular momenta and spin-orbit interaction. *Phys. Rev. L* **2021**, *126*, 243601. [[CrossRef](#)]
29. Hyde, M.W. Twisted space-frequency and space-time partially coherence beam. *Sci. Rep.* **2020**, *10*, 12443. [[CrossRef](#)]
30. Huang, S.L.; Wang, p.; Shen, X.; Liu, J. Properties of the generation and propagation of spatiotemporal optical vortices. *Opt. Express* **2021**, *29*, 26995–27003. [[CrossRef](#)]
31. Mirando, A.; Zang, Y.M.; Zhan, Q.W.; Chong, A. Generation of spatiotemporal optical vortices with partial temporal coherence. *Opt. Express* **2021**, *29*, 30426–30435. [[CrossRef](#)] [[PubMed](#)]
32. Cao, Q.; Chen, J.; Lu, K.Y.; Wan, C.H.; Chong, A.D.; Zhan, Q.W. Sculpturing spatiotemporal wavepackets with chirped pulses. *Photonics Res.* **2021**, *9*, 11002261. [[CrossRef](#)]
33. Ding, C.L.; Horoshko, D.; Korotkova, O.; Jian, C.; Qi, X.X.; Pan, L.Z. Source coherence-induced control of spatiotemporal coherence vortices. *Opt. Express* **2022**, *30*, 19871–19888. [[CrossRef](#)] [[PubMed](#)]

34. Ding, C.; Koivurova, M.; Turunen, J.; Setälä, T.; Friberg, A. Coherence control of pulse trains by spectral phase modulation. *J. Opt.* **2017**, *19*, 095501. [[CrossRef](#)]
35. Zhang, Y.T.; Ding, C.L.; Hyde, W., IV; Korotkova, O. Non-stationary pulses with complex-valued temporal degree of coherence. *J. Opt.* **2020**, *22*, 105607. [[CrossRef](#)]
36. Talukder, R.; Halder, A.; Koivurova, M.; Ding, C.L.; Setälä, T.; Turunen, J.; Friberg, A. Generation of pulse trains with nonconventional temporal correlation properties. *J. Opt.* **2022**, *24*, 055502. [[CrossRef](#)]
37. Mandel, L.; Wolf, E. *Optical Coherence and Quantum Optics*; Cambridge University Press: Cambridge, UK, 1995.

Disclaimer/Publisher's Note: The statements, opinions and data contained in all publications are solely those of the individual author(s) and contributor(s) and not of MDPI and/or the editor(s). MDPI and/or the editor(s) disclaim responsibility for any injury to people or property resulting from any ideas, methods, instructions or products referred to in the content.